

## Article

# Well-Dispersed MgAl<sub>2</sub>O<sub>4</sub> Supported Ni Catalyst with Enhanced Catalytic Performance and the Reason of Its Deactivation for Long-Term Dry Methanation Reaction

Fen Wang <sup>1,2,\*†</sup>, Xiumiao Yang <sup>3,†</sup> and Jingcai Zhang <sup>2</sup>

<sup>1</sup> School of Chemical Engineering, Anhui University of Science and Technology, Huainan 232001, China

<sup>2</sup> Dalian Institute of Chemical Physics, Chinese Academy of Sciences, Dalian 116023, China; zjc@dicp.ac.cn

<sup>3</sup> School of Mechanical Engineering, Anhui University of Science and Technology, Huainan 232001, China; xmyang@aust.edu.cn

\* Correspondence: fenwang@aust.edu.cn; Tel.: +86-13779961290

† These authors contributed equally to this work.

**Abstract:** Dry methanation of syngas is a promising route for synthetic natural gas production because of its water and cost saving characteristics, as we reported previously. Here, we report a simple soaking process for the preparation of well-dispersed Ni/MgAl<sub>2</sub>O<sub>4</sub>-E catalyst with an average Ni size of 6.4 nm. The catalytic test results showed that the Ni/MgAl<sub>2</sub>O<sub>4</sub>-E catalyst exhibited considerably higher activity and better stability than Ni/MgAl<sub>2</sub>O<sub>4</sub>-W catalyst prepared by conventional incipient wetness impregnation method in dry methanation reaction. The long-term stability test result of 335 h has demonstrated that the deactivation of the Ni/MgAl<sub>2</sub>O<sub>4</sub>-E catalyst is inevitable. With multiple characterization techniques including ICP, EDS, XRD, STEM, TEM, SEM and TG, we reveal that the graphitic carbon encapsulating Ni nanoparticles are the major reasons responsible for catalyst deactivation, and the rate of carbon deposition decreases with reaction time.

**Keywords:** dry methanation; Ni/MgAl<sub>2</sub>O<sub>4</sub> catalysts; dispersion; deactivation; carbon deposition



**Citation:** Wang, F.; Yang, X.; Zhang, J. Well-Dispersed MgAl<sub>2</sub>O<sub>4</sub> Supported Ni Catalyst with Enhanced Catalytic Performance and the Reason of Its Deactivation for Long-Term Dry Methanation Reaction. *Catalysts* **2021**, *11*, 1117. <https://doi.org/10.3390/catal11091117>

Academic Editor: Giuseppe Bonura

Received: 27 August 2021

Accepted: 14 September 2021

Published: 16 September 2021

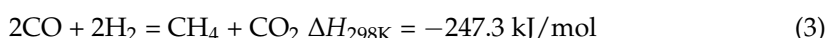
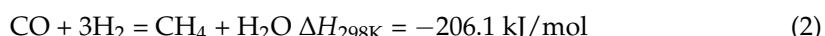
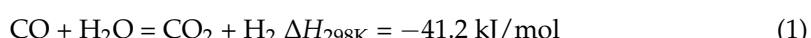
**Publisher's Note:** MDPI stays neutral with regard to jurisdictional claims in published maps and institutional affiliations.



**Copyright:** © 2021 by the authors. Licensee MDPI, Basel, Switzerland. This article is an open access article distributed under the terms and conditions of the Creative Commons Attribution (CC BY) license (<https://creativecommons.org/licenses/by/4.0/>).

## 1. Introduction

The process for direct combustion of coal usually releases many pollutants such as SO<sub>x</sub>, NO<sub>x</sub>, CO<sub>x</sub>, particulate matter (PM), etc., which has resulted in severe environmental pollution [1,2]. Replacing coal with natural gas for combustion can improve the combustion efficiency and significantly minimize pollution because of the high calorific value of natural gas and low emission of pollutants for its combustion. Natural gas import has risen in China in recent years in spite of the emergence of shale gas and combustible ice [3,4]. Therefore, the process of coal to synthetic natural gas has attracted considerable attention in the past [5–7]. Methanation of syngas is a key process for the production of natural gas from coal. Dry methanation of syngas with H<sub>2</sub>/CO ratio of 1 has the advantages of water and cost saving compared with conventional methanation routes due to not needing to adjust the H<sub>2</sub>/CO ratio of raw syngas through water-gas shift (Equation (1)) process before the reaction [8,9]. However, most of the literature focuses on the conventional methanation of syngas with H<sub>2</sub>/CO ratio of 3 (Equation (2)). Dry methanation of syngas with H<sub>2</sub>/CO ratio of 1 has rarely been investigated thus far (Equation (3)).



Nickel based catalysts are most widely used in conventional methanation of syngas with H<sub>2</sub>/CO ratio of 3 or above due to its high activity and low cost [10–13]. Similar to this

conventional methanation reaction, it was found that nickel-based catalysts can efficiently catalyze dry methanation reaction from our previous study [8,9]. It is generally believed that the metallic Ni nanoparticles are the active sites in methanation reaction since the accessible Ni atoms can be reduced by the reducing syngas [14,15]. The main drawback of the Ni catalysts is easily deactivated by production of coke that can affect catalyst lifetime, especially at conditions of a low H<sub>2</sub>/CO ratio. It was reported by many researchers that the presence of highly dispersed small metallic Ni nanoparticles on support can greatly reduce the coking degree [16,17]. Therefore, developing highly dispersed nickel catalysts with small size is highly desirable for dry methanation reaction since it results in an increased surface area of the active phase and a consequent enhancement in the catalytic activity and stability.

Enormous efforts have been devoted to preparing highly dispersed nickel-based catalysts. One way is to develop a suitable catalyst preparation method, such as co-precipitation [18,19], deposition–precipitation [20,21], sol–gel routes [22,23], atomic layer deposition [24,25], etc. He et al. [26] prepared highly dispersed 30.4 wt.% Ni-0.5CeO<sub>2</sub> with Ni crystallite size of 8.4 nm by a co-precipitation method, which is smaller than that of 18.3 wt.% Ni/CeO<sub>2</sub> prepared by incipient wetness impregnation (14.2 nm). Le et al. [27] have reported that the 10 wt.% Ni/Al@Al<sub>2</sub>O<sub>3</sub> catalyst prepared by deposition–precipitation exhibits higher Ni dispersion with Ni particle size of 3–4 nm than that of impregnation catalyst. Lakshmanan et al. [28] synthesized 55 wt.% Ni@SiO<sub>2</sub> core–shell catalyst with Ni mean sizes of 8.0 nm via a sol–gel method, which is far more dispersed than that of 33 wt.% Ni/SiO<sub>2</sub> catalyst with Ni mean sizes of 24.5 nm prepared by a wet impregnation method. Gould et al. [29] reported that Ni/Al<sub>2</sub>O<sub>3</sub> prepared by atomic layer deposition shows higher dispersed Ni nanoparticles as small as 3.0 nm than that of impregnated Ni/Al<sub>2</sub>O<sub>3</sub> with Ni average size of 15 nm. However, several of these preparation methods often require sophisticated operation procedures or strict control of experimental parameters. The sol–gel process involves the use of complex and expensive alkoxide precursors as well as a series of sophisticated operation such as hydrolysis and condensation, etc. [30,31], which always make this method costly and time-consuming. For co-precipitation and deposition–precipitation processes, the pH value of solution should be strictly controlled by adding a basic precipitation agent such as urea, ammonia, NaOH or K<sub>2</sub>CO<sub>3</sub> in the preparation procedure. Otherwise, it will result in the poor reproducibility of catalyst preparation [32,33]. Atomic layer deposition has proven to be a powerful technique for the preparation of highly dispersed Ni catalysts with precise control. However, it suffers from several issues including high precursor cost, low deposition rate and limited scalability, which limit its large-scale commercial application [34–36]. Therefore, it is still necessary to develop a facile approach for synthesis of highly dispersed Ni catalyst.

Magnesium aluminate spinel (MgAl<sub>2</sub>O<sub>4</sub>) has unique optical properties, electrical properties, high melting point (2135 °C), high mechanical strength, chemical inertness and the acceptable catalytic properties. Thus, it has applications in many important areas, such as optically transparent ceramic, neutron radiation resistance, humidity sensors, refractories, catalyst and catalyst support [37,38]. For applications as catalyst support, MgAl<sub>2</sub>O<sub>4</sub> is widely used in a variety of reactions, such as SCR of NO<sub>x</sub>, dehydrogenation reaction, reforming reaction and other type of reactions due to its high thermal stability. In this work, we synthesized a well-dispersed Ni/MgAl<sub>2</sub>O<sub>4</sub>-E catalyst with an average Ni nanoparticle size of 6.4 nm using a facile method. It was found that high activity and stability were achieved on Ni/MgAl<sub>2</sub>O<sub>4</sub>-E catalyst for dry methanation reaction at 400–450 °C, which is superior to that of Ni/MgAl<sub>2</sub>O<sub>4</sub>-W catalyst synthesized by conventional incipient wetness impregnation method. The catalyst structure evolution and deactivation behavior during long-term stability test of 335 h were probed by using ICP, EDS, XRD, STEM, TEM, SEM and TG. We disclosed that the deactivation of Ni/MgAl<sub>2</sub>O<sub>4</sub> catalyst is attributed to the encapsulation of Ni nanoparticles by graphitic carbon.

## 2. Results

### 2.1. Catalyst Characterization

The basic physicochemical characteristics of Ni/MgAl<sub>2</sub>O<sub>4</sub>-W and Ni/MgAl<sub>2</sub>O<sub>4</sub>-E samples are listed in Table 1. The specific surface areas for the Ni/MgAl<sub>2</sub>O<sub>4</sub>-W and Ni/MgAl<sub>2</sub>O<sub>4</sub>-E samples are 242.7 and 220.3 m<sup>2</sup>/g, respectively. It is obvious that the  $S_{\text{BET}}$  values of these two samples have no significant difference. The corresponding pore sizes are 3.5 and 8.6 nm, and the corresponding pore volumes are 0.40 and 0.57 cm<sup>3</sup>/g. The pore sizes were calculated from the desorption branch of the N<sub>2</sub> adsorption–desorption isotherms using the Barrett–Joyner–Halenda (BJH) method. Ni/MgAl<sub>2</sub>O<sub>4</sub>-E has larger pore sizes and pore volumes than Ni/MgAl<sub>2</sub>O<sub>4</sub>-W. It is obvious that the pore size of the Ni/MgAl<sub>2</sub>O<sub>4</sub>-E is the same to that of MgAl<sub>2</sub>O<sub>4</sub> support, while for Ni/MgAl<sub>2</sub>O<sub>4</sub>-W, it is lower than that of MgAl<sub>2</sub>O<sub>4</sub> support. The Ni contents were measured at 5.2 and 4.9 wt.% for the Ni/MgAl<sub>2</sub>O<sub>4</sub>-W and Ni/MgAl<sub>2</sub>O<sub>4</sub>-E samples, respectively, by ICP-OES analysis.

The XRD patterns of Ni/MgAl<sub>2</sub>O<sub>4</sub>-W and Ni/MgAl<sub>2</sub>O<sub>4</sub>-E samples are presented in Figure 1. These two samples show the characteristic diffraction peak of MgAl<sub>2</sub>O<sub>4</sub> spinel (JCPDS 21-1152). Ni/MgAl<sub>2</sub>O<sub>4</sub>-W displays a distinct diffraction peak at 2θ of 51.8°, which is attributed to the (200) plane of metallic Ni (JCPDS 04-0850), while for Ni/MgAl<sub>2</sub>O<sub>4</sub>-E, a broadly weak diffraction peak of metallic Ni at 51.8° is observed. The average crystallite sizes of Ni, which were calculated by using Scherrer equation based on the diffraction of Ni (200), are 9.6 ( $\pm 2.0$ ) and 5.6 ( $\pm 1.4$ ) nm for Ni/MgAl<sub>2</sub>O<sub>4</sub>-W and Ni/MgAl<sub>2</sub>O<sub>4</sub>-E samples, respectively. This result suggests that Ni possesses smaller average size and higher dispersion on MgAl<sub>2</sub>O<sub>4</sub>-E than MgAl<sub>2</sub>O<sub>4</sub>-W.

**Table 1.** Physicochemical characteristics for the Ni/MgAl<sub>2</sub>O<sub>4</sub>-W and Ni/MgAl<sub>2</sub>O<sub>4</sub>-E samples.

Sample	Ni Content (wt.%)	$d_{\text{Ni}}(200)$ (nm)	$S_{\text{BET}}$ (m <sup>2</sup> /g)	Pore Size * (nm)	Pore Volume (cm <sup>3</sup> /g)
MgAl <sub>2</sub> O <sub>4</sub>	-	-	327.6	8.6	0.89
Ni/MgAl <sub>2</sub> O <sub>4</sub> -E	4.9	5.6 ( $\pm 1.4$ )	220.3	8.6	0.57
Ni/MgAl <sub>2</sub> O <sub>4</sub> -W	5.2	9.6 ( $\pm 2.0$ )	242.7	3.5	0.40

\* BJH desorption average pore diameter.

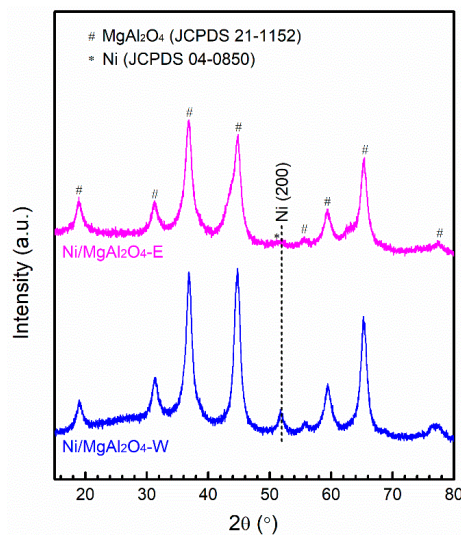


**Figure 1.** XRD patterns for the Ni/MgAl<sub>2</sub>O<sub>4</sub>-W and Ni/MgAl<sub>2</sub>O<sub>4</sub>-E samples.

Figure 2 shows the STEM images of the freshly reduced Ni/MgAl<sub>2</sub>O<sub>4</sub>-W and Ni/MgAl<sub>2</sub>O<sub>4</sub>-E samples. The histograms of Ni particle size distribution for these two samples were obtained by statistical analysis of counting more than 300 Ni particles. Ni/MgAl<sub>2</sub>O<sub>4</sub>-E shows the average Ni nanoparticle size of about 6.4 nm with a narrow

size distribution in the range of 3–11 nm, whereas the Ni/MgAl<sub>2</sub>O<sub>4</sub>-W shows the average Ni nanoparticle size of about 10.1 nm with a wide size distribution in the range of 5–19 nm. The Ni nanoparticle sizes obtained from STEM are well consistent with the ones calculated from XRD data. It indicates that Ni/MgAl<sub>2</sub>O<sub>4</sub>-E has better dispersion of Ni nanoparticles on MgAl<sub>2</sub>O<sub>4</sub> support than Ni/MgAl<sub>2</sub>O<sub>4</sub>-W.

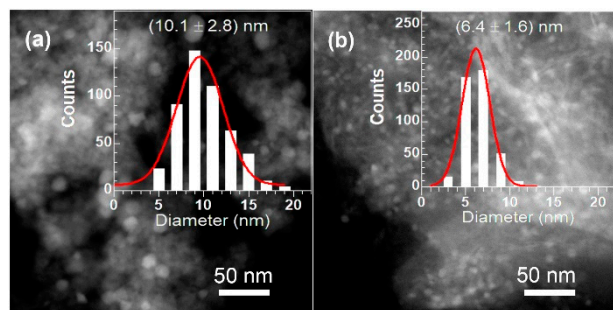


**Figure 2.** STEM images for (a) Ni/MgAl<sub>2</sub>O<sub>4</sub>-W and (b) Ni/MgAl<sub>2</sub>O<sub>4</sub>-E samples.

## 2.2. Catalytic Activity and Stability

We assessed the catalytic performance of the Ni/MgAl<sub>2</sub>O<sub>4</sub>-W and Ni/MgAl<sub>2</sub>O<sub>4</sub>-E catalysts for dry methanation at 0.1 MPa and GHSV of 10,000 mL h<sup>-1</sup> g<sub>cat.</sub><sup>-1</sup>, as shown in Figure 3. The CO conversion ( $X_{CO}$ ) increases from 51.5% to 91.6% when the temperature increases from 350 to 400 °C over Ni/MgAl<sub>2</sub>O<sub>4</sub>-E catalyst. It reaches the equilibrium CO conversion calculated, assuming no carbon formation occurs at 450 °C, and then surpasses them at higher temperatures, while remaining far below the ones calculated, assuming carbon formation occurs, suggesting that carbon formation occurred in the reaction system. Above 450 °C, the  $X_{CO}$  and  $X_{H_2}$  decreases with increasing reaction temperature due to the limitation of chemical equilibrium. The selectivity of CH<sub>4</sub> ( $S_{CH_4}$ ) decreases from 61.9% to 49.6% and then stays at 50–48%, while the selectivity of CO<sub>2</sub> ( $S_{CO_2}$ ) increases from 33.8% to 46.6% and maintains at 47–45% when the temperature increases from 350 to 400 °C and above. The carbon balances are above 95% at all tested temperatures as shown in Table S1. For Ni/MgAl<sub>2</sub>O<sub>4</sub>-W catalyst, when the reaction temperature increases from 350 to 400 °C and above, the  $X_{CO}$  increases from 8.0% to 46.8% and then approaches to the equilibrium conversion calculated, assuming no carbon formation occurs. Meanwhile, the  $S_{CH_4}$  decreases from 74.6% to 52.7% and then holds at 48.1–48.5%, and the  $S_{CO_2}$  increases from 19.0% to 40.5% and then maintains at 47–46%. As a result, CH<sub>4</sub> yields about 45.4% (theoretical yield is 48.2% at 400 °C) and is obtained at 400 °C over Ni/MgAl<sub>2</sub>O<sub>4</sub>-E catalyst. All these above results suggest that Ni/MgAl<sub>2</sub>O<sub>4</sub>-E catalyst shows better catalytic performance for dry methanation reaction than that of Ni/MgAl<sub>2</sub>O<sub>4</sub>-W catalyst.

The effect of gas hourly space velocity (GHSV) on the Ni/MgAl<sub>2</sub>O<sub>4</sub>-E catalyst performance for dry methanation reaction at 450 °C was studied, as shown in Figure 4. With increasing the GHSV, the  $X_{CO}$  starts decreasing from the CO equilibrium conversion (calculated with assuming no carbon formation occurs) when the GHSV is larger than 20,000 mL h<sup>-1</sup> g<sub>cat.</sub><sup>-1</sup>, indicating that mitigation of mass transport limitation begins. Meanwhile, the  $S_{CH_4}$  increases and  $S_{CO_2}$  decreases, consistent with the increase in the difference between  $X_{H_2}$  and  $X_{CO}$ , which reflects that methanation of syngas with H<sub>2</sub>/CO molar ratio above 1, which is pronounced at high GHSV. This requires low GHSV to obtain high  $X_{CO}$  with dry methanation selectivity.

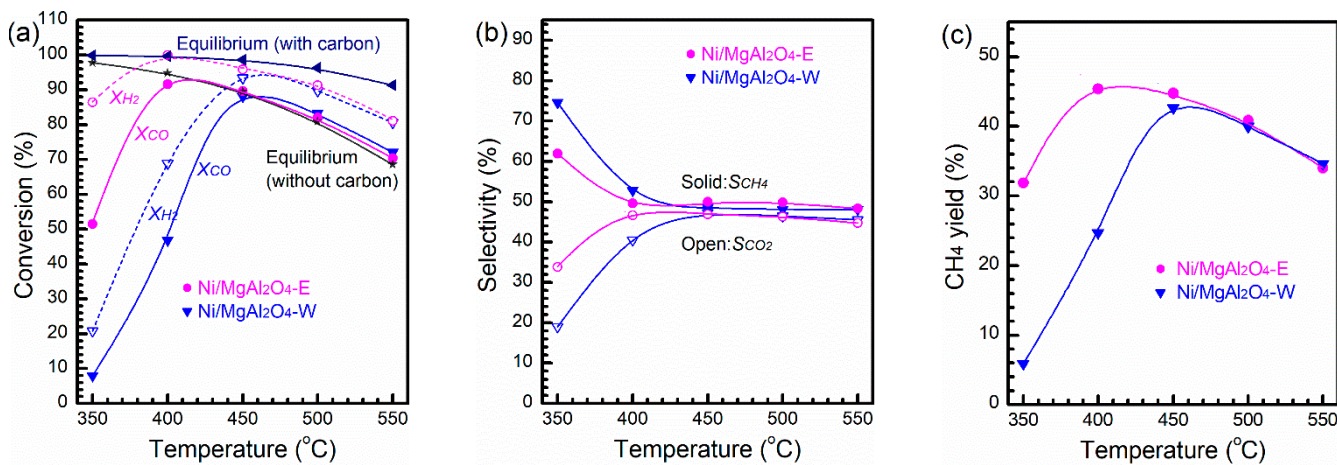


**Figure 3.** (a) Conversion, (b) selectivity and (c) CH<sub>4</sub> yield for dry methanation reaction over Ni/MgAl<sub>2</sub>O<sub>4</sub>-W and Ni/MgAl<sub>2</sub>O<sub>4</sub>-E as a function of reaction temperature at GHSV of 10,000 mL h<sup>-1</sup> g<sub>cat</sub><sup>-1</sup>.

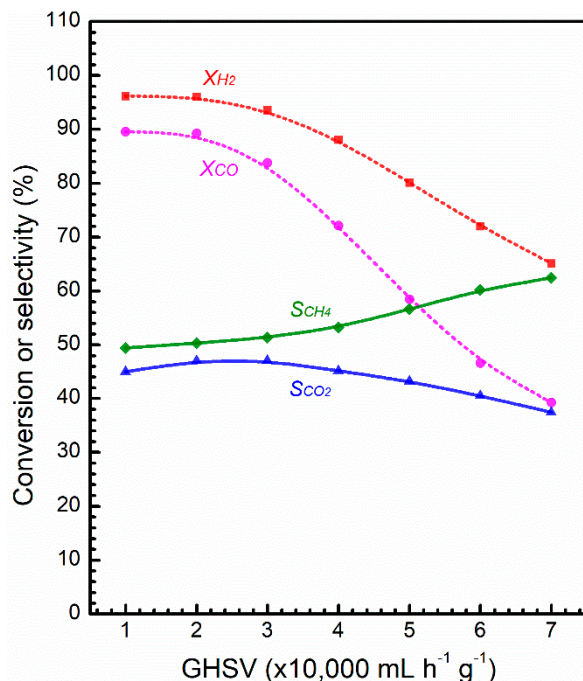


**Figure 4.** Conversions and selectivities over Ni/MgAl<sub>2</sub>O<sub>4</sub>-E as a function of gas hourly space velocity at 450 °C.

Figure 5 shows the catalytic stability results of the Ni/MgAl<sub>2</sub>O<sub>4</sub>-W and Ni/MgAl<sub>2</sub>O<sub>4</sub>-E catalysts in dry methanation reaction at 450 °C with the GHSV of 10,000 mL h<sup>-1</sup> g<sub>cat</sub><sup>-1</sup>. It is obvious that the Ni/MgAl<sub>2</sub>O<sub>4</sub>-E catalyst displays a relatively stable X<sub>CO</sub> of 88–90% during the total test time of 24 h, while the X<sub>CO</sub> over Ni/MgAl<sub>2</sub>O<sub>4</sub>-W decreases from ~90% to 78.2% in the last 16 h of reaction. Both the S<sub>CH<sub>4</sub></sub> and S<sub>CO<sub>2</sub></sub> approach 50% and remain almost unchanged during the total test time because of the high X<sub>CO</sub>, which is also confirmed by the above results (Figures 3 and 4). The above results indicate that Ni/MgAl<sub>2</sub>O<sub>4</sub>-E shows better catalytic stability than Ni/MgAl<sub>2</sub>O<sub>4</sub>-W catalyst.

The catalytic stability of the Ni/MgAl<sub>2</sub>O<sub>4</sub>-E catalyst in dry methanation reaction was further investigated by the long-term test at 450 °C and GHSV of 10,000 mL h<sup>-1</sup> g<sub>cat</sub><sup>-1</sup>. As shown in Figure 6, the X<sub>CO</sub> continuously decreases from 91.1% to 18.4% during 300 h time on stream (TOS). It decreases by 6.5%, 10.8%, 12.1% and 17.5% in the first four consecutive 50 h periods, respectively, displaying increasing deactivation rates. The S<sub>CH<sub>4</sub></sub> increases from 50.6% to 60.5% and S<sub>CO<sub>2</sub></sub> decreases from 47.9% to 26.1% along with the decrease of

$X_{CO}$  in similar ways to that presented in Figure 4. After reaction, significant coke in the catalyst bed is visible. After burning coke with air and reducing the spent catalyst with  $H_2$  at  $650\text{ }^{\circ}\text{C}$ , the regenerated catalyst exhibits initial  $X_{CO}$  of 86.0% and  $S_{CH_4}$  and  $S_{CO_2}$  of 50.6% and 47.2%, respectively. However, the  $X_{CO}$  decreases dramatically to 43.8% within 24 h TOS and the  $S_{CH_4}$  and  $S_{CO_2}$  turn to 60.4% and 41.2%, indicating that irreversible deterioration of the catalyst occurs probably due to coke combustion.

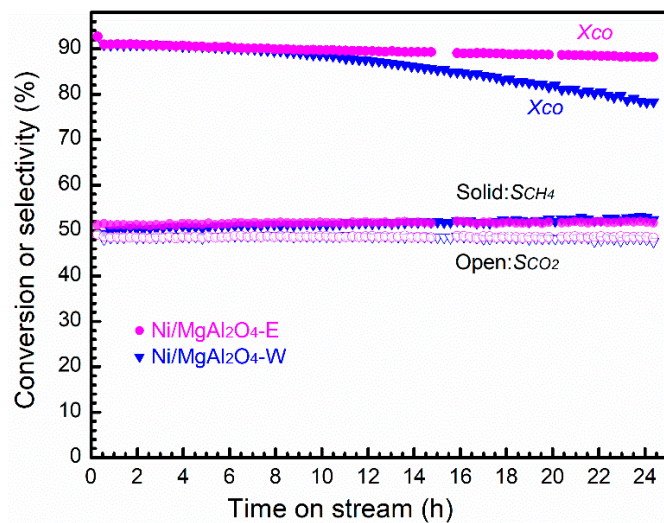


**Figure 5.** The stability results of the  $\text{Ni}/\text{MgAl}_2\text{O}_4\text{-W}$  and  $\text{Ni}/\text{MgAl}_2\text{O}_4\text{-E}$  catalysts in dry methanation reaction at  $450\text{ }^{\circ}\text{C}$  and GHSV of  $10,000\text{ mL h}^{-1}\text{ g}_{\text{cat.}}^{-1}$ .

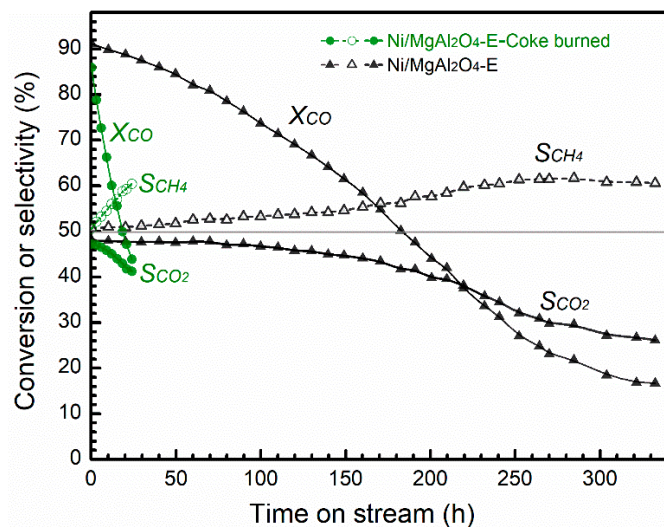


**Figure 6.** Long-term stability result of the  $\text{Ni}/\text{MgAl}_2\text{O}_4\text{-E}$  catalyst in dry methanation reaction at  $450\text{ }^{\circ}\text{C}$  and GHSV of  $10,000\text{ mL h}^{-1}\text{ g}_{\text{cat.}}^{-1}$ .

A series of characterization techniques were used to probe the structure evolution of the  $\text{Ni}/\text{MgAl}_2\text{O}_4\text{-E}$  catalyst in the long-term stability test. Figure 7 shows the STEM images for the  $\text{Ni}/\text{MgAl}_2\text{O}_4\text{-E}$  catalyst after different reaction times at reaction conditions of  $450\text{ }^{\circ}\text{C}$  and  $10,000\text{ mL h}^{-1}\text{ g}_{\text{cat.}}^{-1}$ . The average Ni nanoparticle sizes of the  $\text{Ni}/\text{MgAl}_2\text{O}_4\text{-E}$  after reaction for 5 and 150 h are 6.9 and 6.4 nm, respectively (Figure 7a,b), which show similar sizes as that of the fresh one (Figure 2b). The average Ni nanoparticle size for the regenerative catalyst of  $\text{Ni}/\text{MgAl}_2\text{O}_4\text{-E}$  increases to 11.5 nm, and the Ni nanoparticles with large sizes of 25–35 nm are clearly observed because of presumed deterioration of the catalyst (the insert image of Figure 7c). These results are in good accord with the sizes calculated by Scheer equation using the XRD data (Table S2 and Figure S1). The

obvious increase for the Ni nanoparticle size of the regenerative catalyst may explain the phenomenon of its fast deactivation in dry methanation reaction.

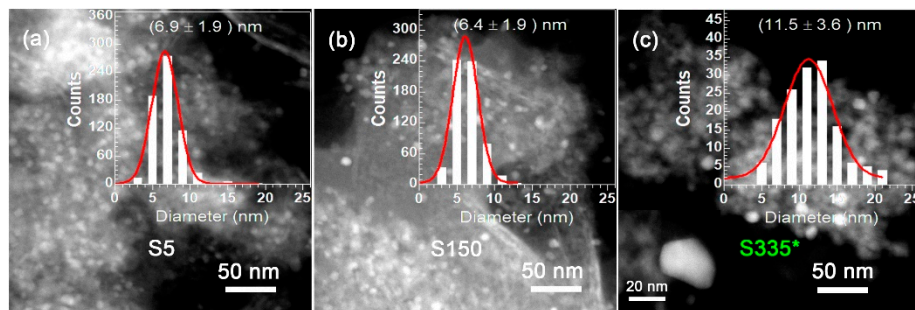


**Figure 7.** STEM images for the spent Ni/MgAl<sub>2</sub>O<sub>4</sub>-E catalyst: (a) Ni/MgAl<sub>2</sub>O<sub>4</sub>-S5, (b) Ni/MgAl<sub>2</sub>O<sub>4</sub>-S150 and (c) Ni/MgAl<sub>2</sub>O<sub>4</sub>-S335\*.

TEM images reveal the massive deposits of carbon for the spent catalyst, which has a filamentous structure with a Ni nanoparticle attached to the end (Figure 8b–d). HRTEM images display that the graphitic carbon encapsulated the Ni nanoparticles as shown in a representative sample of S150 (Figure 8c). The measured d-spacing values of the graphitic carbon is 0.34 nm, which is the well-crystallized graphitic carbon (JCPDS 75-1621) and is also verified by XRD crystallography (Figure S1). SEM images of the spent catalysts also show the formation of filamentous carbon deposits with Ni nanoparticles at their tips (Figure S2a–c). The deposits of carbon over Ni/MgAl<sub>2</sub>O<sub>4</sub>-S150 were completely removed by regeneration operation (Figure S2d). The amount of carbon deposits over spent catalysts was measured by thermogravimetric (TG) analysis during temperature-programmed oxidation. The weight losses of the spent catalysts below 350 °C are attributed to the desorption of the physiosorbed water, as we previously reported, for the similar types of catalysts. The weight losses of Ni/MgAl<sub>2</sub>O<sub>4</sub>-S5, Ni/MgAl<sub>2</sub>O<sub>4</sub>-S10, Ni/MgAl<sub>2</sub>O<sub>4</sub>-S50, Ni/MgAl<sub>2</sub>O<sub>4</sub>-S150 and Ni/MgAl<sub>2</sub>O<sub>4</sub>-S335\* are 4.5%, 5.0%, 13.6%, 28.3% and 11.4%, respectively, in the temperature range of 350 and 650 °C, which is associated with the oxidation of carbon deposits during temperature programmed processes (Table S2 and Figure S3) [9]. The amount of carbon deposits with reaction time over spent catalysts obtained from TG data are presented in Figure 9a. It is obvious that the longer reaction times give rise to more deposits of carbon. Notably, the amount of carbon deposits over Ni/MgAl<sub>2</sub>O<sub>4</sub>-S335 were obtained by recording the weight of reactor before and after reaction. Figure 9b shows the relationship between the average accumulation rate of carbon deposits over Ni/MgAl<sub>2</sub>O<sub>4</sub>-E and the reaction time. It demonstrates clearly that the accumulation rate of carbon deposits decreases with the increase of reaction time.

In order to check whether the amount of Ni over Ni/MgAl<sub>2</sub>O<sub>4</sub>-E is loss under reaction condition, the Ni content of the Ni/MgAl<sub>2</sub>O<sub>4</sub>-E catalyst after different reaction time was determined by ICP and EDS analysis. The Ni content of Ni/MgAl<sub>2</sub>O<sub>4</sub>-S5, Ni/MgAl<sub>2</sub>O<sub>4</sub>-S10, Ni/MgAl<sub>2</sub>O<sub>4</sub>-S50, Ni/MgAl<sub>2</sub>O<sub>4</sub>-S150 and Ni/MgAl<sub>2</sub>O<sub>4</sub>-S335\* determined by ICP is 4.9, 5.0, 5.0, 5.2, and 5.1 wt.%, respectively (Table S2). The EDS for elemental analysis further reveals that the Ni content of Ni/MgAl<sub>2</sub>O<sub>4</sub>-S335\* is 4.9 wt.% (Figure S4), which is well consistent with the results obtained from ICP test. These results suggest that the Ni content of Ni/MgAl<sub>2</sub>O<sub>4</sub>-E catalyst hardly changes during the long-term stability test under reaction condition.

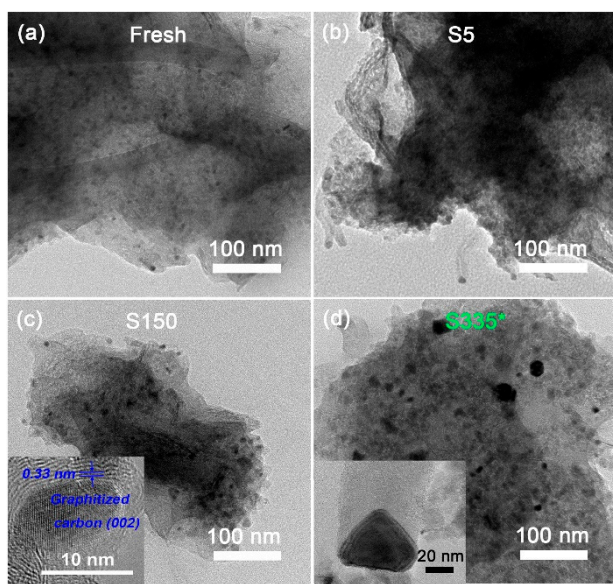


**Figure 8.** TEM images for the fresh and spent Ni/MgAl<sub>2</sub>O<sub>4</sub>-E catalyst: (a) fresh catalyst, (b) after reaction for 5 h, (c) after reaction for 150 h, and (d) after reaction for 335 h followed by regeneration and reaction for 24 h.

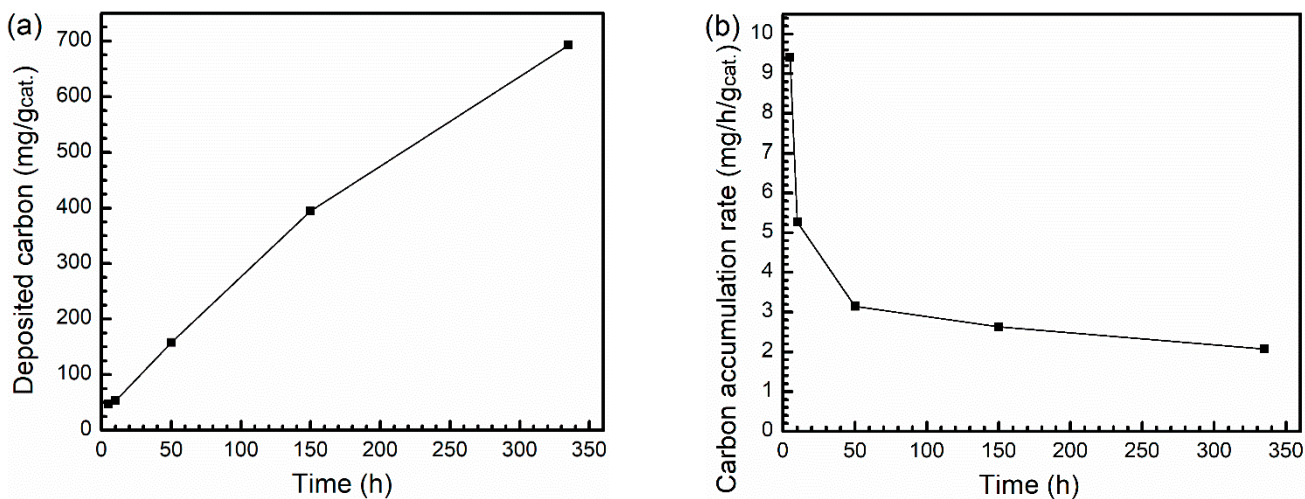


**Figure 9.** (a) The amount of carbon deposits over Ni/MgAl<sub>2</sub>O<sub>4</sub>-E catalyst after different reaction time and (b) the average accumulation rate of carbon deposits as a function of reaction time over Ni/MgAl<sub>2</sub>O<sub>4</sub>-E catalyst.

### 3. Discussion

Ni/MgAl<sub>2</sub>O<sub>4</sub>-E catalyst shows higher activity and better stability than that of Ni/MgAl<sub>2</sub>O<sub>4</sub>-W catalyst in dry methanation reaction at 450 °C and GHSV of 10,000 mL h<sup>-1</sup> g<sub>cat</sub>.<sup>-1</sup> (Figures 3 and 5). According to the ICP results, these two catalysts have similar Ni content of ~5 wt.-% (Table 1). XRD crystallography and STEM images reveal that the Ni/MgAl<sub>2</sub>O<sub>4</sub>-E catalyst shows higher dispersion of Ni with the average particle size of ~6 nm, while the Ni/MgAl<sub>2</sub>O<sub>4</sub>-W catalyst exhibits lower dispersion of Ni with the average particle size of ~10 nm (Table 1, Figures 1 and 2). According to the literature, the amount of deposited coke increases with the size of Ni nanoparticles increasing from ~6 to ~10 nm [39]. These are the possible reasons for the large difference in catalytic performance for dry methanation reaction over Ni/MgAl<sub>2</sub>O<sub>4</sub>-W and Ni/MgAl<sub>2</sub>O<sub>4</sub>-E catalysts.

However, Ni/MgAl<sub>2</sub>O<sub>4</sub>-E catalyst deactivation is still inevitable during the 335 h long-term stability test in dry methanation at 450 °C and GHSV of 10,000 mL h<sup>-1</sup> g<sub>cat</sub>.<sup>-1</sup> (Figure 6). No meaningful change for the morphology and particle size of Ni after the

stability test for different time was observed according to the XRD and STEM results (Figures 1 and 7). From the TEM images and SEM images, obvious filamentous carbon with a nickel crystallite attached to the end formed over Ni/MgAl<sub>2</sub>O<sub>4</sub>-E catalyst after the stability test for different times (Figure 8 and Figure S2). HRTEM images reveal that the Ni nanoparticles were encapsulated by the graphitic carbon. Moreover, considerably more carbon deposits formed with longer stability test time, as evidenced by TG results (Table S2 and Figures 9a and S3). In addition, the Ni content of the Ni/MgAl<sub>2</sub>O<sub>4</sub>-E after the stability test for different time does not (or hardly) change, including under the reaction atmosphere of high CO concentration, as determined by ICP and EDS analysis (Table S2 and Figure S4). The catalytic activity of the deactivated Ni/MgAl<sub>2</sub>O<sub>4</sub>-E cannot be fully recovered by regeneration, which is probably due to the increased Ni particle size during regeneration process (Table S2 and Figures 7c and 8d). All these above results indicate that carbon deposition is the main reason for the deactivation of the Ni/MgAl<sub>2</sub>O<sub>4</sub>-E catalyst in dry methanation reaction.

## 4. Materials and Methods

### 4.1. Catalyst Preparation

MgAl<sub>2</sub>O<sub>4</sub> support was synthesized by a solvothermal method, as we previously reported [9,40] and then was calcined at 600 °C for 5 h. Ni/MgAl<sub>2</sub>O<sub>4</sub>-E was prepared by soaking MgAl<sub>2</sub>O<sub>4</sub> support powder in absolute ethanol solution of Ni(NO<sub>3</sub>)<sub>2</sub>·6H<sub>2</sub>O ( $\geq 98.0\%$ , Damao, Tianjin, China) with continuous stirring for 24 h at room temperature. The obtained mixture was filtered and dried at 110 °C for 11 h, and then calcined at 350 °C for 5 h with a heating rate of 5 °C/min. The calcined sample was further reduced at 700 °C for 2 h under pure hydrogen followed with passivation in 1 vol.% O<sub>2</sub>/N<sub>2</sub> at room temperature for 2 h with a flow rate of 20 mL/min before exposure to air. Ni/MgAl<sub>2</sub>O<sub>4</sub>-W was prepared by conventional incipient wetness impregnation of MgAl<sub>2</sub>O<sub>4</sub> support with aqueous solution of Ni(NO<sub>3</sub>)<sub>2</sub>·6H<sub>2</sub>O. The impregnated sample was then dried, calcined, reduced and passivated under the same condition as that of Ni/MgAl<sub>2</sub>O<sub>4</sub>-E. The spent Ni/MgAl<sub>2</sub>O<sub>4</sub>-E catalysts after 5, 10, 50, 150, and 335 h reaction were denoted as Ni/MgAl<sub>2</sub>O<sub>4</sub>-S5, Ni/MgAl<sub>2</sub>O<sub>4</sub>-S10, Ni/MgAl<sub>2</sub>O<sub>4</sub>-S50, Ni/MgAl<sub>2</sub>O<sub>4</sub>-S150 and Ni/MgAl<sub>2</sub>O<sub>4</sub>-S335, respectively. The spent Ni/MgAl<sub>2</sub>O<sub>4</sub>-E catalyst after 335 h reaction and regeneration and then after 24 h reaction was denoted as Ni/MgAl<sub>2</sub>O<sub>4</sub>-S335\*. The spent catalysts were regenerated by burning coke at 650 °C for 0.5 h in an air flow of 20 mL/min and then reduction at 650 °C for 2 h in a H<sub>2</sub> flow of 40 mL/min.

### 4.2. Catalyst Characterization

The specific surface areas, pore size and pore volume of the samples were measured at −196 °C on a Micromeritics ASAP 2460 instrument (Norcross, GA, USA). All samples were degassed at 350 °C for 5 h under vacuum prior to the adsorption measurements. The Ni loading of the samples was determined by inductively coupled plasma optical emission spectroscopy (ICP-OES, Waltham, MA, USA). X-ray diffraction (XRD) patterns of the samples were recorded on an X-ray diffractometer (PANalytical PW 3040/60 X'Pert PRO, Almelo, The Netherlands) with a Cu K $\alpha$  ( $\lambda = 0.154$  nm) radiation source at 40 kV and 40 mA. The micro-morphologies of the samples were characterized on a scanning electron microscopy (JEOL JSM-7800F, Tokyo, Japan). All the samples were grinded into powder and coated onto a conductive tape before characterization. TEM and STEM images were obtained on a transmission electronic microscopy (JEM-2100F, Tokyo, Japan) with a high-angle annular dark field scanning transmission electron microscopy (HAADF-STEM, Tokyo, Japan) detector. Energy dispersive X-ray spectroscopy (EDS) analysis was performed on an adjacent ISIS/INCA energy dispersive X-ray spectrometer (Oxford Instruments, Oxford, UK) equipped with an ultrathin window (UTW) detector. The amount of carbon deposits on the spent catalysts were measured using a thermogravimetric analyzer (TA instrument, SDT Q600, New Castle, DE, USA) by temperature programmed oxidation method with a heating rate of 10 °C/min in an air flow of 100 mL/min.

#### 4.3. Catalytic Performance Tests

Dry methanation reaction tests were performed in a fixed-bed quartz tubular reactor (i.d. = 10 mm) at atmosphere pressure. For each test, all the catalysts powders were diluted with 2 g of quartz sand and then loaded into a U-shaped reactor. The reactant gases consisted of 48 vol.% CO, 48 vol.% H<sub>2</sub> and 4 vol.% N<sub>2</sub> (internal standard). The flow rates of reactant gases were controlled by mass flow controllers and the reaction temperature was controlled by a programmable temperature controller with a K-type thermocouple. The products and unconverted reactants at the reactor outlet were analyzed using an online gas chromatography (Agilent 7890B, Santa Clara, CA, USA) equipped with a thermal conductivity detector (TCD, Santa Clara, CA, USA) and two packed columns (Parapak N and 5A molecular sieve). The CO and H<sub>2</sub> conversion were calculated as  $X_i = (n_{i,in} - n_{i,out})/n_{i,in}$ , where  $i$  is CO and H<sub>2</sub>. The CH<sub>4</sub> and CO<sub>2</sub> selectivity were calculated as  $S_j = n_{j,out}/(n_{CO,in} - n_{CO,out})$ , where  $j$  is CH<sub>4</sub> and CO<sub>2</sub>. The carbon balance was calculated as the moles of carbon at the reactor outlet divided by the moles of carbon at the reactor inlet.

#### 5. Conclusions

In this work, we report that the well-dispersed Ni/MgAl<sub>2</sub>O<sub>4</sub>-E catalyst with smaller average size of Ni nanoparticles shows better catalytic performance than the Ni/MgAl<sub>2</sub>O<sub>4</sub>-W catalyst in dry methanation reaction under the studied reaction conditions. High and stable catalytic performance was obtained at 400–450 °C over Ni/MgAl<sub>2</sub>O<sub>4</sub>-E catalyst. However, Ni/MgAl<sub>2</sub>O<sub>4</sub>-E catalyst deactivation is inevitable during the long-term stability test at 450 °C due to the encapsulation of Ni nanoparticles by the graphitic carbon. The regeneration of catalyst did not recover the performance of Ni/MgAl<sub>2</sub>O<sub>4</sub>-E catalyst, most likely owing to the increase of Ni nanoparticles size in the process of burning coke. We will focus on the research of exploring suitable regeneration operations condition and designing anti-coking catalysts in the future.

**Supplementary Materials:** The following are available online at <https://www.mdpi.com/article/10.3390/catal11091117/s1>, Figure S1: XRD patterns for the spent Ni/MgAl<sub>2</sub>O<sub>4</sub>-E catalysts, Table S1: CO conversions, product selectivities and carbon balances for dry methanation reaction over Ni/MgAl<sub>2</sub>O<sub>4</sub>-E catalyst at different temperatures with GHSV of 10,000 mL h<sup>-1</sup> g<sub>cat</sub><sup>-1</sup>, Figure S2: SEM images for the spent Ni/MgAl<sub>2</sub>O<sub>4</sub>-E catalysts: (a) Ni/MgAl<sub>2</sub>O<sub>4</sub>-S50, (b) Ni/MgAl<sub>2</sub>O<sub>4</sub>-S150, (c) Ni/MgAl<sub>2</sub>O<sub>4</sub>-S335\* and (d) after reaction for 150 h followed by regeneration. Table S2: Metallic Ni content, metallic Ni and graphitic carbon crystallite size and weight loss during TG of Ni/MgAl<sub>2</sub>O<sub>4</sub>-E catalyst after different reaction time. Figure S3: TG results for the spent Ni/MgAl<sub>2</sub>O<sub>4</sub>-E catalysts, Figure S4: STEM-EDS images for the Ni/MgAl<sub>2</sub>O<sub>4</sub>-S335\* catalyst.

**Author Contributions:** Investigation, F.W., X.Y. and J.Z.; supervision, F.W. and X.Y.; data curation, F.W. and X.Y.; writing—original draft preparation, F.W. and X.Y.; writing—review and editing, F.W. and J.Z.; funding acquisition, F.W. and X.Y. All authors have read and agreed to the published version of the manuscript.

**Funding:** This research was funded by the Anhui Provincial Natural Science Foundation (2108085QB49), the Scientific Research Foundation for the Introduction of Talent, Anhui University of Science and Technology (13200001) and the University-level General Projects of Anhui University of Science and Technology (xjyb2020-07).

**Data Availability Statement:** Not applicable.

**Conflicts of Interest:** The authors declare no conflict of interest.

#### References

1. Rahmaninejad, F.; Gavaskar, V.S.; Abbasian, J. Dry regenerable CuO/γ-Al<sub>2</sub>O<sub>3</sub> catalyst for simultaneous removal of SO<sub>x</sub> and NO<sub>x</sub> from flue gas. *Appl. Catal. B Environ.* **2012**, *119–120*, 297–303. [[CrossRef](#)]
2. Zhang, Y.; Schauer, J.J.; Zhang, Y.; Zeng, L.; Wei, Y.; Liu, Y.; Shao, M. Characteristics of particulate carbon emissions from real-world Chinese coal combustion. *Environ. Sci. Technol.* **2008**, *42*, 5068–5073. [[CrossRef](#)]
3. Zhang, Q.; Li, Z.; Wang, G.; Li, H. Study on the impacts of natural gas supply cost on gas flow and infrastructure deployment in China. *Appl. Energy* **2016**, *162*, 1385–1398. [[CrossRef](#)]

4. Ding, Y.; Han, W.; Chai, Q.; Yang, S.; Shen, W. Coal-based synthetic natural gas (SNG): A solution to China's energy security and CO<sub>2</sub> reduction? *Energy Policy* **2013**, *55*, 445–453. [[CrossRef](#)]
5. Gao, L.; Fu, Q.; Wei, M.; Zhu, Y.; Liu, Q.; Crumlin, E.; Liu, Z.; Bao, X. Enhanced Nickel-catalyzed methanation confined under hexagonal boron nitride shells. *ACS Catal.* **2016**, *6*, 6814–6822. [[CrossRef](#)]
6. Shinde, V.M.; Madras, G. CO methanation toward the production of synthetic natural gas over highly active Ni/TiO<sub>2</sub> catalyst. *AIChE J.* **2014**, *60*, 1027–1035. [[CrossRef](#)]
7. Ren, J.; Li, H.; Jin, Y.; Zhu, J.; Liu, S.; Lin, J.; Li, Z. Silica/titania composite-supported Ni catalysts for CO methanation: Effects of Ti species on the activity, anti-sintering, and anti-coking properties. *Appl. Catal. B Environ.* **2017**, *201*, 561–572. [[CrossRef](#)]
8. Wang, F.; Zhang, J.; Chen, Z.; Lin, J.; Li, W.; Wang, Y.; Chen, B. Water-saving dry methanation for direct conversion of syngas to synthetic natural gas over robust Ni<sub>0.1</sub>Mg<sub>0.9</sub>Al<sub>2</sub>O<sub>4</sub> catalyst. *J. Catal.* **2019**, *375*, 466–477. [[CrossRef](#)]
9. Wang, F.; Zhang, J.; Li, W.; Chen, B. Coke-resistant Au–Ni/MgAl<sub>2</sub>O<sub>4</sub> catalyst for direct methanation of syngas. *J. Energy Chem.* **2019**, *39*, 198–207. [[CrossRef](#)]
10. Lebarbier, V.M.; Dagle, R.A.; Kovarik, L.; Albrecht, K.O.; Li, X.; Li, L.; Taylor, C.E.; Bao, X.; Wang, Y. Sorption-enhanced synthetic natural gas (SNG) production from syngas: A novel process combining CO methanation, water-gas shift, and CO<sub>2</sub> capture. *Appl. Catal. B Environ.* **2014**, *144*, 223–232. [[CrossRef](#)]
11. Gao, J.; Jia, C.; Zhang, M.; Gu, F.; Xu, G.; Su, F. Effect of nickel nanoparticle size in Ni/α-Al<sub>2</sub>O<sub>3</sub> on CO methanation reaction for the production of synthetic natural gas. *Catal. Sci. Technol.* **2013**, *3*, 2009–2015. [[CrossRef](#)]
12. Li, J.; Li, P.; Li, J.; Tian, Z.; Yu, F. Highly-dispersed Ni-NiO nanoparticles anchored on an SiO<sub>2</sub> support for an enhanced CO methanation performance. *Catalysts* **2019**, *9*, 506. [[CrossRef](#)]
13. Kim, T.; Jo, S.; Lee, Y.; Kang, S.; Kim, J.; Lee, S.; Kim, J. Influence of Ni on Fe and Co-Fe based catalysts for high-calorific synthetic natural gas. *Catalysts* **2021**, *11*, 697. [[CrossRef](#)]
14. Du, G.; Lim, S.; Yang, Y.; Wang, C.; Pfefferle, L.; Haller, G.L. Methanation of carbon dioxide on Ni-incorporated MCM-41 catalysts: The influence of catalyst pretreatment and study of steady-state reaction. *J. Catal.* **2007**, *249*, 370–379. [[CrossRef](#)]
15. Czekaj, I.; Loviat, F.; Raimondi, F.; Wambach, J.; Biollaz, S.; Wokaun, A. Characterization of surface processes at the Ni-based catalyst during the methanation of biomass-derived synthesis gas: X-ray photoelectron spectroscopy (XPS). *Appl. Catal. A Gen.* **2007**, *329*, 68–78. [[CrossRef](#)]
16. Kim, J.-H.; Suh, D.J.; Park, T.-J.; Kim, K.-L. Effect of metal particle size on coking during CO<sub>2</sub> reforming of CH<sub>4</sub> over Ni-alumina aerogel catalysts. *Appl. Catal. A Gen.* **2000**, *197*, 191–200. [[CrossRef](#)]
17. Zhan, Y.; Song, K.; Shi, Z.; Wan, C.; Pan, J.; Li, D.; Au, C.; Jiang, L. Influence of reduction temperature on Ni particle size and catalytic performance of Ni/Mg(Al)O catalyst for CO<sub>2</sub> reforming of CH<sub>4</sub>. *Int. J. Hydrg. Energy* **2020**, *45*, 2794–2807. [[CrossRef](#)]
18. Jung, Y.; Yoon, W.; Seo, Y.; Rhee, Y. The effect of precipitants on Ni-Al<sub>2</sub>O<sub>3</sub> catalysts prepared by a co-precipitation method for internal reforming in molten carbonate fuel cells. *Catal. Commun.* **2012**, *26*, 103–111. [[CrossRef](#)] [[PubMed](#)]
19. Liu, H.; Chen, T.; Chang, D.; Chen, D.; Kong, D.; Zou, X.; Frost, R.L. Effect of preparation method of palygorskite-supported Fe and Ni catalysts on catalytic cracking of biomass tar. *Chem. Eng. J.* **2012**, *188*, 108–112. [[CrossRef](#)]
20. Liu, J.; Li, C.; Wang, F.; He, S.; Chen, H.; Zhao, Y.; Wei, M.; Evans, D.G.; Duan, X. Enhanced low-temperature activity of CO<sub>2</sub> methanation over highly-dispersed Ni/TiO<sub>2</sub> catalyst. *Catal. Sci. Technol.* **2013**, *3*, 2627–2633. [[CrossRef](#)]
21. Bitter, J.H.; van der Lee, M.K.; Slotboom, A.G.T.; van Dillen, A.J.; de Jong, K.P. Synthesis of highly loaded highly dispersed nickel on carbon nanofibers by homogeneous deposition–precipitation. *Catal. Lett.* **2003**, *89*, 139–142. [[CrossRef](#)]
22. Wu, C.; Williams, P.T. A novel nano-Ni/SiO<sub>2</sub> catalyst for hydrogen production from steam reforming of ethanol. *Environ. Sci. Technol.* **2010**, *44*, 5993–5998. [[CrossRef](#)]
23. Zhang, W.D.; Liu, B.S.; Zhan, Y.P.; Tian, Y.L. Syngas production via CO<sub>2</sub> reforming of methane over Sm<sub>2</sub>O<sub>3</sub>–La<sub>2</sub>O<sub>3</sub>-supported Ni catalyst. *Ind. Eng. Chem. Res.* **2009**, *48*, 7498–7504. [[CrossRef](#)]
24. Jiang, C.; Shang, Z.; Liang, X. Chemosselective transfer hydrogenation of nitroarenes catalyzed by highly dispersed, supported nickel nanoparticles. *ACS Catal.* **2015**, *5*, 4814–4818. [[CrossRef](#)]
25. Zhang, J.; Chen, C.; Yan, W.; Duan, F.; Zhang, B.; Gao, Z.; Qin, Y. Ni nanoparticles supported on CNTs with excellent activity produced by atomic layer deposition for hydrogen generation from the hydrolysis of ammonia borane. *Catal. Sci. Technol.* **2016**, *6*, 2112–2119. [[CrossRef](#)]
26. He, L.; Liang, B.; Li, L.; Yang, X.; Huang, Y.; Wang, A.; Wang, X.; Zhang, T. Cerium-oxide-modified nickel as a non-noble metal catalyst for selective decomposition of hydrous hydrazine to hydrogen. *ACS Catal.* **2015**, *5*, 1623–1628. [[CrossRef](#)]
27. Le, T.A.; Kim, J.; Kang, J.K.; Park, E.D. CO and CO<sub>2</sub> methanation over Ni/Al@Al<sub>2</sub>O<sub>3</sub> core–shell catalyst. *Catal. Today* **2020**, *356*, 622–630. [[CrossRef](#)]
28. Lakshmanan, P.; Kim, M.S.; Park, E.D. A highly loaded Ni@SiO<sub>2</sub> core–shell catalyst for CO methanation. *Appl. Catal. A Gen.* **2016**, *513*, 98–105. [[CrossRef](#)]
29. Gould, T.D.; Lubers, A.M.; Neltner, B.T.; Carrier, J.V.; Weimer, A.W.; Falconer, J.L.; Will Medlin, J. Synthesis of supported Ni catalysts by atomic layer deposition. *J. Catal.* **2013**, *303*, 9–15. [[CrossRef](#)]
30. Hench, L.L.; West, J.K. The sol-gel process. *Chem. Rev.* **1990**, *90*, 33–72. [[CrossRef](#)]
31. Xiao, Z.; Ma, Z.; Wang, X.; Williams, C.T.; Liang, C. Effects of synthetic parameters on the structure and catalytic performance of Cu–Cr catalysts prepared by a non-alkoxide sol–gel route. *Ind. Eng. Chem. Res.* **2011**, *50*, 2031–2039. [[CrossRef](#)]

32. Hakeem, A.A.; Zhao, Z.; Kapteijn, F.; Makkee, M. Revisiting the synthesis of Au/TiO<sub>2</sub> P25 catalyst and application in the low temperature water–gas shift under realistic conditions. *Catal. Today* **2015**, *244*, 19–28. [[CrossRef](#)]
33. Wolf, A.; Schüth, F. A systematic study of the synthesis conditions for the preparation of highly active gold catalysts. *Appl. Catal. A Gen.* **2002**, *226*, 1–13. [[CrossRef](#)]
34. Leskelä, M.; Ritala, M. Atomic layer deposition chemistry: Recent developments and future challenges. *Angew. Chem. Int. Edit.* **2003**, *42*, 5548–5554. [[CrossRef](#)] [[PubMed](#)]
35. Han, B.; Lang, R.; Qiao, B.; Wang, A.; Zhang, T. Highlights of the major progress in single-atom catalysis in 2015 and 2016. *Chin. J. Catal.* **2017**, *38*, 1498–1507. [[CrossRef](#)]
36. Liu, J. Catalysis by supported single metal atoms. *ACS Catal.* **2017**, *7*, 34–59. [[CrossRef](#)]
37. Ganesh, I. A review on magnesium aluminate (MgAl<sub>2</sub>O<sub>4</sub>) spinel: Synthesis, processing and applications. *Int. Mater. Rev.* **2013**, *58*, 63–112. [[CrossRef](#)]
38. Seeman, V.; Feldbach, E.; Kärner, T.; Maaroos, A.; Mironova-Ulmane, N.; Popov, A.I.; Shablonin, E.; Vasil'chenko, E.; Lushchik, A. Fast-neutron-induced and as-grown structural defects in magnesium aluminate spinel crystals with different stoichiometry. *Opt. Mater.* **2019**, *91*, 42–49. [[CrossRef](#)]
39. Luisetto, I.; Tuti, S.; Battocchio, C.; Mastro, S.L.; Sodo, A. Ni/CeO<sub>2</sub>–Al<sub>2</sub>O<sub>3</sub> catalysts for the dry reforming of methane: The effect of CeAlO<sub>3</sub> content and nickel crystallite size on catalytic activity and coke resistance. *Appl. Catal. A Gen.* **2015**, *500*, 12–22. [[CrossRef](#)]
40. Wang, F.; Li, W.; Lin, J.; Chen, Z.; Wang, Y. Crucial support effect on the durability of Pt/MgAl<sub>2</sub>O<sub>4</sub> for partial oxidation of methane to syngas. *Appl. Catal. B Environ.* **2018**, *231*, 292–298. [[CrossRef](#)]